

Homogenization of composite materials reinforced with unidirectional fibres with complex curvilinear cross section: a virtual element approach

E. Artioli ¹, G. Elefante ² A. Sommariva² and M. Vianello ²

¹ Engineering Department “Enzo Ferrari”
University of Modena and Reggio Emilia
edoardo.artioli@unimore.it

² Department of Mathematics “Tullio Levi-Civita”
University of Padova
{elefante, alvise, marcov}@math.unipd.it

June 3, 2024

Abstract

The paper presents an augmented curvilinear virtual element method to determine homogenized in-plane shear material moduli of long-fibre reinforced composites in the framework of asymptotic homogenization method. The new virtual element combine an exact representation of the curvilinear computational geometry for complex fibre cross section shapes through an innovative two-dimensional cubature suite for NURBS-like polygonal domains. A selection of representative numerical tests supports the accuracy and efficiency of the proposed approach for both doubly periodic and random fibre arrangement with matrix domain.

2010 AMS subject classification: 65D07, 65D10, 65D17, 65D18, 65D32, 65N30.

Keywords: material homogenization, fibre reinforced composite, low-cardinality algebraic cubature, PI (Positive Interior) rules, curvilinear polygons, NURBS, Virtual Element Method.

1 Introduction

The use of composite materials for engineering applications is a continuously broadening field, due to their high performances under several points of view. Many are in fact the advantages offered by such materials, as for instance lighter weight, the ability to tailor layup for optimum strength and stiffness, improved

fatigue life, corrosion resistance, and, through good design practice, reduced assembly costs due to fewer detail parts and fasteners. For these reasons these composites are used in several fields of engineering, for example in civil engineering are used for strengthening of reinforced concrete columns, in mechanical engineering in high performance racing cars, aerospace and biomechanical applications being as well a growing network in this regard. A special class in this realm is represented by fibre-reinforced composite materials. The specific strength of superior quality material fibres (especially carbon, glass, metal alloy, just to mention a few types) are higher than those of embedding matrices making these materials an interesting option for the construction of numerous technical devices. Being intrinsically heterogeneous, deriving homogenized equivalent material properties is mandatory in design practice. Amongst the many different methods developed in recent years, asymptotic homogenization has become widely known and quite popular due to the versatility in application with respect to material configuration of fibre and matrix arrangements. The method nonetheless requires a numerical approximation whenever the geometry of fibres or their disposition within the surrounding matrix becomes complex, being classical FE methods the usual tool in this context.

A powerful alternative to FEM and inherent limitations, is offered by the Virtual Element Method (VEM), a recently introduced numerical method for approximation of PDEs [8, 7] which can be viewed as an extension of Finite Element Methods to general polygonal and polyhedral elements. The strongest aspects in favor of the VEM are its firm mathematical foundations, simplicity in implementation, and efficiency and accuracy in computations, as well as mesh adaptivity together with the possibility of having curvilinear polygonal meshes. The latter aspect in particular results quite efficient in the study of the overall mechanical behavior of fibre-reinforced composite materials through homogenization since the ensuing boundary value (cell) problem is posed, in general, on curvilinear domains bounded by material interfaces identified on the cross section orthogonal plane [5].

This work presents a curvilinear VEM approach for the computational homogenization of in-plane shear moduli for unidirectional fibre reinforced materials having inclusions with complex shape profiles. A key point of the procedure relies on an efficient 2D cubature algorithm for NURBS boundary polygons which grants positive weights and interior nodes. An extensive campaign of numerical applications illustrate accuracy and convergence patterns of the method, both for doubly periodic regular arrangements of fibres and for randomly distributed fibres within the matrix phase.

The paper is organized as follows: Section 2 presents the governing equations of the considered homogenization problem, Section 3 introduces the curvilinear VEM approximation space and the discretized form of the problem. Sections 4-7 are devoted to the cubature formula for NURBS-shaped curvilinear polygons. Last, Section 8 presents a set of selected numerical tests supporting the accuracy and efficiency of the proposed methodology. Conclusions are drawn in Section 9.

2 Asymptotic homogenization of fibre-reinforced composite: the anti-plane problem

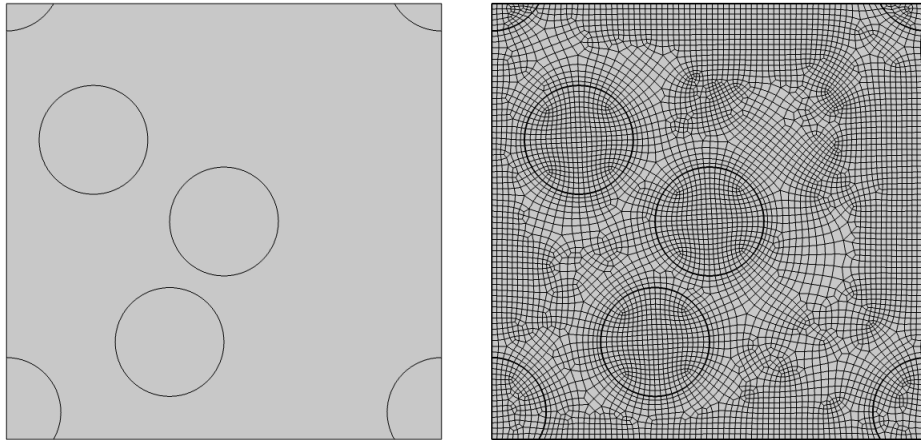


Figure 1: Stochastic realization of a square-shaped repeating unit cell (RUC) of a composite with volume fraction $f = 0.2$ and four circular fibres (*left panel*). Conforming curvilinear quadrilateral mesh (*right panel*).

This section is devoted to a unified compact presentation of the so called computational asymptotic homogenization of antiplane shear moduli for both a doubly-periodic or a random fibre-reinforced composite. We consider a composite material, reinforced with long, parallel fibres, distributed in the material with a statistically homogeneous microstructure, given either by a doubly periodic or a random spatial arrangement. Fibres have all same cross section with a possibly complex shape: in the present context we assume that the curvilinear curve defining the boundary for a given cross section is described through a single NURBS or a C^0 regular blend of subsequent NURBS curves.

In either case, at microscale, the section orthogonal to fibres is represented by a doubly-periodic arrangement of repeating unit cells (RUC). A RUC is a parallelogram, having edges L_1 , L_2 , and an angle φ , containing a given number F of fibres, as represented in Fig. 1 for the two exemplary cases of doubly periodic and random type of composite. A given material setup is characterized by the so called volume fraction, denoted by $f = \sum_{j=1}^F f_j$ which represents the ratio between fibre material area and RUC total area.

The case studied in this communication refers to effective *in-plane* elastic shear moduli, which are computed applying computational asymptotic homogenization through Virtual Element Method, due to a lack of closed-form solutions

of the aforementioned problem for fibres with complex cross section boundary. Statement of the problem is given by the following set of boundary value problems of equilibrium over the composite cross section domain:

$$\operatorname{div}(\mathbf{G}\nabla w_\varepsilon) = 0, \quad \text{in } \cup_j \Omega_{j\varepsilon}^f \cup \Omega_\varepsilon^m; \quad (1)$$

$$\llbracket \mathbf{G}\nabla w_\varepsilon \cdot \boldsymbol{\nu} \rrbracket = 0, \quad \text{on } \cup_j \Gamma_{j\varepsilon}; \quad (2)$$

$$\mathbf{G}\nabla w_\varepsilon \cdot \boldsymbol{\nu} = \frac{1}{\varepsilon} D_j \llbracket w_\varepsilon \rrbracket, \quad \text{on } \cup_j \Gamma_{j\varepsilon}. \quad (3)$$

indexed by a parameter ε . In the above, w_ε denotes the displacement field in the fibre axes direction, and $\cup_j \Omega_{j\varepsilon}^f$ and Ω_ε^m indicate fibres and matrix domains, respectively, while $\cup_j \Gamma_{j\varepsilon}$ is defined as the set of all fibre/matrix interfaces, and $\boldsymbol{\nu}$ represents the unit normal to $\cup_j \Gamma_{j\varepsilon}$ towards Ω_ε^m . The double square brackets operator $\llbracket \cdot \rrbracket$ denotes jump across the fibre interface, defined as extra-minus-intra difference. Parameter ε is a scaling factor for the microstructure, such that $\varepsilon = 1$ corresponds to the actual composite material, while homogenization limit is reached for the limit of ε approaching zero.

The physical meaning of the above set of governing equations is as follows: Equation (1) represents translational equilibrium along fibre axis direction; Eq. (2) represents in-plane equilibrium at fibre/matrix interface i.e. continuity of the normal-to-interface shear stress component; Eq. (3) is actually a constitutive equation, also known as linear spring-layer model [23, 21], ruling the zero-thickness imperfect interface behavior in terms of displacement jump $\llbracket w_\varepsilon \rrbracket$ and normal traction $\mathbf{G}\nabla w_\varepsilon \cdot \boldsymbol{\nu}$ at the interface in such a way that parameter(s) D_j are selected to represent the level of interface degradation [12]. Lastly, factor ε^{-1} provides the right scaling for the homogenization limit [23].

Assuming homogeneous isotropic linear elastic fibre and matrix material behavior, the in-plane effective shear moduli, which are collected by the constitutive tensor \mathbf{G} , are given by:

$$\mathbf{G} = \mathbf{G}_j^f = G^f \mathbf{I} \quad \text{in } \Omega_{j\varepsilon}^f, \quad j = 1 \dots F, \quad (4)$$

$$\mathbf{G} = \mathbf{G}^m = G^m \mathbf{I} \quad \text{in } \Omega_\varepsilon^m. \quad (5)$$

where \mathbf{I} is the unit tensor. An interesting generalization for fibres to incorporate cylindrical orthotropy, with material grading along the radial direction, could be also taken into account for the particular case of circular fibres (see [3] for more details), but it is here omitted for simplicity.

Well posedness of the homogenization problem requires the following conditions to hold:

$$G^m > 0, \quad G^f > 0, \quad D_j > 0, \quad j = 1 \dots F. \quad (6)$$

where G^m , G^f are shear moduli, for the matrix and the fibre, respectively, D_j is the fibre/matrix interface elastic stiffness parameter (see Eq. (3)).

2.1 Homogenization of in-plane shear moduli

To derive the homogenized or effective in-plane shear moduli of the composite material, asymptotic homogenization shall be employed herein. With reference

to a given RUC, the procedure identifies two characteristic separate length scales for the spatial domain under consideration, i.e. two different space variables: a macroscopic one, x , and a microscopic one, $y = x/\varepsilon$, $y \in \mathbf{D}$, being \mathbf{D} the RUC (see Fig. 1), whose extra-fibre space, intra-fibre space and fibre-matrix interface are denoted by \mathbf{D}^m , \mathbf{D}_j^f and Γ_j , for $j = 1 \dots F$, respectively. Thence, an asymptotic expansion of the primary variable, the axial displacement field, is considered with respect to powers of ε :

$$w_\varepsilon(x, y) = w_0(x, y) + \varepsilon w_1(x, y) + \varepsilon^2 w_2(x, y) + \dots, \quad (7)$$

where w_0 , w_1 , w_2 are doubly periodic functions over the RUC domain, with w_1 , w_2 having zero integral average over \mathbf{D} . Substituting this expansion in the equilibrium form Eqs. (1)–(3) and equating the power-like terms of ε , a set of three differential problems for w_0 , w_1 and w_2 , respectively are obtained, which in turn lead (see [11, 29]) to the homogenized equilibrium equation for the so called macroscopic displacement w_0 :

$$\operatorname{div}_x(\mathbf{G}^\# \nabla_x w_0) = 0. \quad (8)$$

where $\nabla_x w_0$ is a macroscopic shear strain, and

$$\mathbf{G}^\# = \frac{1}{|\mathbf{D}|} \int_{\mathbf{D}} \mathbf{G}(\mathbf{I} - \nabla_y^t \boldsymbol{\chi}) \, da \quad (9)$$

is the *effective* constitutive tensor. In the above, the superscript t stands for a transpose, da is the area element on \mathbf{D} , $|\cdot|$ the Lebesgue measure. Function $\boldsymbol{\chi}(y)$ which is introduced as the *cell function* has components χ_s , $s = 1, 2$, which represents the unique, null average, \mathbf{D} -periodic solutions of the cell problem:

$$\operatorname{div}_y[\mathbf{G}(\nabla_y \chi_s - \mathbf{e}_s)] = 0, \quad \text{in } \mathbf{D}^f \cup \mathbf{D}^m; \quad (10)$$

$$\llbracket \mathbf{G}(\nabla_y \chi_s - \mathbf{e}_s) \cdot \boldsymbol{\nu} \rrbracket = 0, \quad \text{on } \cup_j \Gamma_j; \quad (11)$$

$$\mathbf{G}(\nabla_y \chi_s - \mathbf{e}_s) \cdot \boldsymbol{\nu} = D_j \llbracket \chi_s \rrbracket, \quad \text{on } \cup_j \Gamma_j, \quad (12)$$

where \mathbf{e}_s is the unit vector parallel to the y_s axis.

Using Gauss-Green Lemma and introducing an *auxiliary cell function*:

$$\tilde{\boldsymbol{\chi}}(y_1, y_2) = \boldsymbol{\chi}(y_1, y_2) - (y_1 \mathbf{e}_1 + y_2 \mathbf{e}_2), \quad (13)$$

the following expression for the effective material moduli is obtained:

$$\mathbf{G}^\# = \mathbf{G}^m + \frac{1}{|\mathbf{D}|} \sum_{j=1}^F \int_{\mathbf{D}_j^f} (\operatorname{div}_y \mathbf{G}^f) \otimes \tilde{\boldsymbol{\chi}} \, da + \frac{1}{|\mathbf{D}|} \sum_{j=1}^F \int_{\Gamma_j} \llbracket \mathbf{G} \boldsymbol{\nu} \otimes \tilde{\boldsymbol{\chi}} \rrbracket \, dl, \quad (14)$$

with dl line element on Γ_j . Eq. (14) is indeed applied to compute $\mathbf{G}^\#$ in terms of $\tilde{\boldsymbol{\chi}}$.

2.2 Weak form

The cell problem (10)-(12) is usually rephrased in weak form through virtual work fundamental identity:

$$\begin{cases} \text{Find } \tilde{\chi}_s \in \tilde{\mathbf{V}} \text{ such that} \\ a(\tilde{\chi}_s, \delta\chi_s) = 0 \quad \forall \delta\chi_s \in \mathbf{V}, s = 1, 2 \end{cases} \quad (15)$$

where $\tilde{\mathbf{V}} := H_{sp}^1(\mathbf{D})$ is the space of admissible auxiliary cell functions $\tilde{\chi}$ which are RUC-shifted D-periodic vector valued functions satisfying: (13))

$$\chi_s(y_1 + L_1, y_2) = \chi_s(y_1, y_2) = \chi_s(y_1 + L_2 \cos \varphi, y_2 + L_2 \sin \varphi). \quad (16)$$

In a functional space setting:

$$\tilde{\mathbf{V}} = \left\{ \tilde{\chi} \in L^2(\mathbf{D}) \text{ such that } \tilde{\chi}|_{\mathbf{D}_j^f} \in H^1(\mathbf{D}_j^f) \text{ for } j = 1, 2, \dots, F, \right. \\ \left. \tilde{\chi}|_{\mathbf{D}^m} \in H^1(\mathbf{D}^m), \tilde{\chi}(y_1, y_2) + y_s \text{ satisfies (16), } s = 1, 2 \right\}.$$

Indicating \mathbf{V} the space of the admissible D-periodic variations of $\tilde{\mathbf{V}}$, the bilinear form associated with the stress divergence term results:

$$a(\tilde{\chi}_s, \delta\chi_s) = - \int_{\mathbf{D}} \text{div}_y[\mathbf{G}(\nabla_y \tilde{\chi}_s)] \delta\chi_s \, \mathbf{d}\mathbf{x} \quad (17)$$

which, applying Gauss-Green lemma, using the interface elastic law (12) and observing the outward normals to fibre and matrix domains at their interface are mutually opposite, becomes:

$$\begin{aligned} a(\tilde{\chi}_s, \delta\chi_s) &= \int_{\mathbf{D}^m} \nabla_y \delta\chi_s \cdot \mathbf{G}^m(\nabla_y \tilde{\chi}_s) \, \mathbf{d}\mathbf{x} + \sum_{j=1}^F \int_{\mathbf{D}_j^f} \nabla_y \delta\chi_s \cdot \mathbf{G}_j^f(\nabla_y \tilde{\chi}_s) \, \mathbf{d}\mathbf{x} \\ &+ \sum_{j=1}^F \int_{\Gamma_j} [[\delta\chi_s]] D_j [[\tilde{\chi}_s]] \, dl. \end{aligned} \quad (18)$$

or, in a more general fashion:

$$a(\tilde{\chi}_s, \delta\chi_s) = \int_{\mathbf{D}} \nabla_y \delta\chi_s \cdot \mathbf{G}(\nabla_y \tilde{\chi}_s) \, \mathbf{d}\mathbf{x} + \sum_{j=1}^F \int_{\Gamma_j} [[\delta\chi_s]] D_j [[\tilde{\chi}_s]] \, dl. \quad (19)$$

The form $a(\cdot, \cdot)$ is symmetric, continuous and coercive on $\tilde{\mathbf{V}}$, so that problem (15) is well posed.

3 Lowest order augmented curvilinear virtual element method

A virtual element discretization of problem (15) for curvilinear polygons is here presented, much along the general idea outlined in [10]. Denote \mathcal{T}_h as a *simple*

polygonal mesh on D , i.e. any decomposition of D in a finite set of simple polygons E , without holes and with boundary given by a finite number of edges. In this realm, and for the forthcoming application, we will primarily focus on meshes of quadrilaterals, given their simplicity, efficiency and wide possibility of generation through conventional mesh generators. For a curvilinear element with one or more edges lying on a fibre/matrix interface Γ_j , we shall describe its geometry in exact form as long as it can be recovered by a NURBS representation (cf. Section 4). Hence, the proposed methodology offers a wide feasibility in terms of fibre cross section boundary shapes allowing for complex profiles in this regard. Any given interface Γ_j is then intended as a NURBS parametrization i.e. an invertible C^1 mapping with proper weights and control points or a C^1 blend of NURBS curves such that any portion is explicitly computable. Dropping index j to lighten up notation, we simply indicate

$$\gamma : [0, L] \longrightarrow \Gamma$$

to indicate a generic curved part of the fibre/matrix interface Γ with the relevant NURBS representation.

Remark 3.1 *In what follows we denote with e any edge of the mesh and with ν a generic vertex. The symbol h will be associated with a length quantity, hence h_E denotes the diameter of element E and h_e the length of a (possibly curved) edge e . As usual, the maximum mesh element size is indicated by h with no subscripts.*

3.1 The augmented virtual element space

For the discretization of the cell problem which is required to compute the effective shear moduli, we propose a simple, computationally efficient enrichment of the VEM space proposed in [10], for lowest order discretization $k = 1$, coupled with a NURBS like representation of curvilinear polygons abutting the material interfaces between fibres and matrix. Given a (curvilinear) polygon $E \in \mathcal{T}_h$ with some edge laying on a curved interface Γ_j ($j \in \{1, 2, \dots, F\}$), for any such curved edge e , we denote with $\gamma_e : [a, b] \rightarrow e$ the restriction of the parametrization for Γ_j to edge e . Then we indicate the standard space of \mathbb{R}^2 polynomials of degree k restrictions on edge e as

$$\tilde{\mathcal{P}}_k(e) = \left\{ p(\gamma_e) : p \in \mathcal{P}_k(\mathbb{R}^2) \right\}.$$

The local virtual element space on E is then defined introducing the space of traces on a curved edge as follows. For a given integer $k \geq 1$, on a given element E with a curved edge γ , we consider the trace space

$$B_h(\partial E) = \left\{ v \in C^0(\partial E) \text{ such that } : v|_e \in \mathcal{P}_k(e) \forall \text{ straight edge } e \subset \partial E, \right. \\ \left. \text{and } v|_\gamma \in \tilde{\mathcal{P}}_k(e) \forall \text{ curved edge } e \subset \partial E \right\}. \quad (20)$$

Then, for every integer $k \geq 1$ the local virtual element space is defined as

$$\mathbf{V}_h(E) = \left\{ v \text{ such that } v|_{\partial E} \in B_h(\partial E), \Delta v \in \mathcal{P}_{k-2}(E) \right\}. \quad (21)$$

For $k = 1$, which is the primarily investigated case of the present contribution, the selected degrees of freedom of the local space are (cf. [10])

- pointwise evaluation at each vertex of E ;
- one extra single degree of freedom for any given curved edge.

Note that the investigated case $k = 1$ amounts to a number of local degrees of freedom which equates the classical curvilinear case (cf. [5]) plus only one extra dof for the curved edge on the polygon. **Fig. 2 illustrates the choice of the additional node on the curved edge, associated to the extra degree of freedom in the augmented form for the relevant case $k = 1$ which simply amounts to adding an extra node for any given curvilinear element edge.** In passing we note that, owing to interelement continuity, this node is shared by both curved elements abutting such an edge. The global conforming space is obtained by a

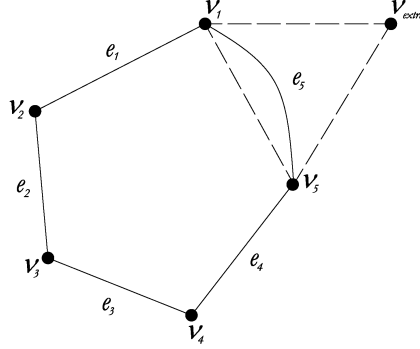


Figure 2: **Typical curvilinear virtual element (case $k = 1$) at fibre matrix curved interface boundary. Case with curved edge no. 5 equipped with additional degree of freedom (node v_{extra}).**

standard identification of degrees of freedom, i.e. as the unique values at the interelement, gluing local spaces with C^0 regularity:

$$\tilde{\mathbf{V}}_h = \left\{ v \in \tilde{\mathbf{V}} : v|_E \in \mathbf{V}_h(E) \forall E \in \mathcal{T}_h \right\},$$

The same holds for the spaces of discrete variations:

$$\mathbf{V}_h = \left\{ v \in \mathbf{V} : v|_E \in \mathbf{V}_h(E) \forall E \in \mathcal{T}_h \right\}.$$

3.2 Discretization of the problem

The discretization of the problem is an augmented combination of the scheme proposed in [10] for the case with straight and curvilinear edges and the original method introduced in [9] for curvilinear VEM; the projection space for virtual cell functions is here augmented with an additional deformation mode at no extra cost in terms of local degrees of freedom.

We propose here an *augmented* projection operator, local to element E , which represents an approximated cell function component χ_s ($s = 1, 2$) which is explicitly computable. Denote with (\tilde{x}, \tilde{y}) the usual shifted centroidal Cartesian coordinates at element level. Let $[\mathcal{P}_{\text{aug}}(E)]$ be the set of polynomials spanned by the monomials $\{1, \tilde{x}, \tilde{y}, \tilde{x}\tilde{y}\}$ (hence linears augmented by the skew-symmetric monomial $\tilde{x}\tilde{y}$) restricted to E . Given $E \in \mathcal{T}_h$ and any $v_h \in \mathbf{V}_h(E)$, the operator $\Pi^\nabla : \mathbf{V}_h(E) \rightarrow [\mathcal{P}_{\text{aug}}(E)]$ is defined by

$$\begin{cases} \int_{\partial E} \Pi^\nabla(v_h) ds = \int_{\partial E} v_h ds \\ \int_E \nabla \Pi^\nabla(v_h) \cdot \nabla \mathbf{p}_{\text{aug}} dE = \int_E \nabla(v_h) \cdot \nabla \mathbf{p}_{\text{aug}} dE \quad \forall \mathbf{p}_{\text{aug}} \in [\mathcal{P}_{\text{aug}}(E)], \end{cases}$$

where $\nabla(v_h)$ denotes the gradient of v_h with respect to y_s ($s = 1, 2$) at the microscale. Hence, the augmented projector $\Pi^\nabla(v_h)$ is an extension of the standard L^2 projection of v_h on $[\mathcal{P}_1(E)]$ since, at the price of the same number of local degrees of freedom of the standard $k = 1$ case, the approximated cell function belongs to a polynomial space which is larger than the standard one, encompassing also the quadratic skew-symmetric monomial term $\tilde{x}\tilde{y}$. This case is indeed quite relevant from the point of view of accuracy, since many RUC geometrical and material arrangements lead to a skew-symmetric solution of the homogenized equilibrium problem in terms of cell function χ_s . It is immediate to check that the above operator $\Pi^\nabla(v_h)$ is readily computable through integration by parts and using the adopted degrees of freedom, see [8, 7, 10] for the relevant standard derivations.

The aforementioned integrals and all the quantities relevant to post processing of the solution (namely the homogenized material moduli) are computed for NURBS curvilinear polygons with the efficient quadrature formula outlined in Section 4.

Once the projector is defined, the development of the VEM method proceeds by deriving the local discrete counterpart of the bulk term in the bilinear form (19) as follows. For an $E \in \mathcal{T}_h$, for all $v_h, w_h \in \mathbf{V}_h(E)$, we define:

$$a_h^E(v_h, w_h) = \int_E \nabla \Pi^\nabla(w_h) \cdot \mathbf{G} \nabla \Pi^\nabla(v_h) dE + s^E((I - \pi \Pi^\nabla)v_h, (I - \pi \Pi^\nabla)w_h) \quad (22)$$

where the first term is a direct approximation of $\int_E \nabla w_h \cdot \mathbf{G}(\nabla v_h)$ by substituting ∇ with $\nabla \Pi^\nabla$, and the second term is a stabilization term of the $dof_i - dof_i$ type (see [24] for a thorough discussion of the subject and possible variants). To this end, an additional operator $\pi : \mathbf{V}_h(E) \rightarrow \mathcal{P}_1(E)$ on linear monomials

is introduced (given the relevant simplicity in coding), defined as the unique minimizer of the euclidean norm distance of the degrees of freedom values with respect to such polynomial space canonical basis. The stabilization form is then taken as:

$$s^E((I-\pi\Pi^\nabla)v_h, (I-\pi\Pi^\nabla)w_h) = \alpha_E \sum_{i=1}^{\#dofs} \left(\text{dof}_i(w_h - \pi\Pi^\nabla w_h) \right) \left(\text{dof}_i(v_h - \pi\Pi^\nabla v_h) \right) \quad (23)$$

where the dof_i symbol denotes evaluation at the i^{th} local degree of freedom and the positive scalar α_E is introduced to ensure physical dimension consistency with the previous term. The present choice is indeed $\alpha_E = \text{trace}(\mathbf{G})/2$. More details on the stabilization can be found for instance in [24].

The global discrete equilibrium equation at microscale over a RUC domain then reads:

$$a_h(v_h, w_h) = \sum_{E \in \mathcal{T}_h} a_h^E(v_h, w_h) + \sum_{j=1}^F \int_{\Gamma_j} \llbracket w_h \rrbracket D_j \llbracket v_h \rrbracket dl$$

for any v_h, w_h in $\tilde{\mathbf{V}}_h$ or \mathbf{V}_h . Note that the jumps in the above expression do not imply any computational issue since the virtual cell function and their variations are explicit at the element boundaries.

The proposed Virtual Element Method then reads

$$\begin{cases} \text{Find } \tilde{\chi}_{hs} \in \tilde{\mathbf{V}}_h \text{ such that} \\ a_h(\tilde{\chi}_{hs}, \delta\chi_{hs}) = 0 \quad \forall \delta\chi_{hs} \in \mathbf{V}_h, s = 1, 2. \end{cases} \quad (24)$$

The above construction and the ensuing post-processing heavily relies on integrating known functions over the polygonal domain which can present NURBS-like curved edges. In the following section we detail the proposed efficient quadrature formula adopted throughout our numerical simulation campaign.

4 Numerical cubature over rational spline curvilinear polygons

In this section we sketch the details on the computation of numerical rules over piecewise rational spline curvilinear polygons, following the details introduced in [35].

In particular we consider Jordan domains $\mathcal{S} \subset \mathbb{R}^2$

1. whose boundary $\partial\mathcal{S}$ is described by parametric equations $x = \tilde{x}(t)$, $y = \tilde{y}(t)$, $t \in [a, b]$, $\tilde{x}, \tilde{y} \in C([a, b])$, $\tilde{x}(a) = \tilde{x}(b)$ and $\tilde{y}(a) = \tilde{y}(b)$;
2. for which there are partitions $\{I^{(k)}\}_{k=1, \dots, M}$ of $[a, b]$, and $\{I_j^{(k)}\}_{j=1, \dots, m_k}$ of each $I^{(k)} \equiv [t^{(k)}, t^{(k+1)}]$, such that the restrictions of \tilde{x}, \tilde{y} on each closed interval $I^{(k)}$ are *rational splines*, w.r.t. the subintervals $\{I_j^{(k)}\}_{j=1, \dots, m_k}$.

We adopt as notation

$$\tilde{x}(t) = \frac{u_{k,1}(t)}{v_{k,1}(t)}, \quad \tilde{y}(t) = \frac{u_{k,2}(t)}{v_{k,2}(t)}, \quad t \in I^{(k)}, \quad (25)$$

being $u_{k,1}, u_{k,2}, v_{k,1}, v_{k,2}$ splines on $I^{(k)}$, sharing the same knots and having degree, respectively, $\eta_{k,1}, \eta_{k,2}, \delta_{k,1}, \delta_{k,2}$, $k = 1, \dots, M$.

Notice, that since $\tilde{x}, \tilde{y} \in C([a, b])$, we are assuming that the denominators $v_{k,1}, v_{k,2}$, $k = 1, \dots, M$ are everywhere not null in the closed interval $I^{(k)}$.

In what follows we intend to show some examples of domains that fulfill these requests.

First, this is the case of a spline curvilinear region as those presented in [36].

Indeed, let $V_k = (\tilde{x}(t_k), \tilde{y}(t_k)) \in \mathbb{R}^2$, $k = 1, \dots, M$, $V_{M+1} = V_1$, be the *vertices* of such a Jordan domain \mathcal{S} , then $\partial\mathcal{S} := \cup_{k=1}^M V_k \cap V_{k+1}$ and each curvilinear side $V_k \cap V_{k+1}$ can be tracked by a parametric spline of degree δ_k , interpolating an ordered subsequence of knots $P_{1,k} = V_k, P_{2,k}, \dots, P_{m_k-1,k}, P_{m_k,k} = V_{k+1}$ with a suitable parametrization determining each $I_j^{(k)}$ (and thus each $I^{(k)}$).

Another large family of domains \mathcal{S} belonging to the class defined above is when $\partial\mathcal{S}$ is a *composite Bezier closed curve*, whose k -th component is of the form

$$\mathcal{B}(\tilde{t}) = \mathcal{B}(\omega_k(t)) = \sum_{i=0}^{m_k-1} b_{i,m_k-1}(t) P_{i+1,k},$$

where $\tilde{t} = \frac{t^{(k+1)} + t^{(k)}}{2} + \frac{t^{(k+1)} - t^{(k)}}{2} t := \omega_k(t)$, $t \in [0, 1]$ and

$$b_{i,l}(t) = \binom{l}{i} t^i (1-t)^{l-i}, \quad i = 0, \dots, l-1, \quad t \in [0, 1]$$

are the *Bernstein polynomials*.

The framework also includes domains whose boundary $\partial\mathcal{S}$ is locally a p -th degree NURBS curve [26, p.117], where the k -th curvilinear side $V_k \cap V_{k+1}$ takes the form

$$C(t) = \frac{\sum_{i=1}^{m_k} B_{i,p}(t) \lambda_{i,k} P_{i,k}}{\sum_{i=1}^{m_k} B_{i,p}(t) \lambda_{i,k}}, \quad t \in [t^{(k)}, t^{(k+1)}]$$

where

- $\{P_{i,k}\}_{i=1}^{m_k}$ are the *control points*,
- $\{\lambda_{i,k}\}_{i=1}^{m_k}$ are the *weights*,
- $\{B_{i,p}\}_{i=1}^{m_k}$ are the p -th degree B-spline basis functions [14, p.87] defined on the nonperiodic (and nonuniform) knot vector

$$U = \underbrace{\{t^{(k)}, \dots, t^{(k)}\}}_{p+1}, t_{p+1}^{(k)}, \dots, t_{m_k-(p+1)}^{(k)}, \underbrace{\{t^{(k+1)}, \dots, t^{(k+1)}\}}_{p+1}.$$

with $t_{p+j}^{(k)} \leq t_{p+j+1}^{(k)}$, $j = 1, \dots, m_k - 1$.

Some classical examples are domains whose boundary is given by a polygon in which a side is substituted by a circular or ellipse arc (see Fig. 3).

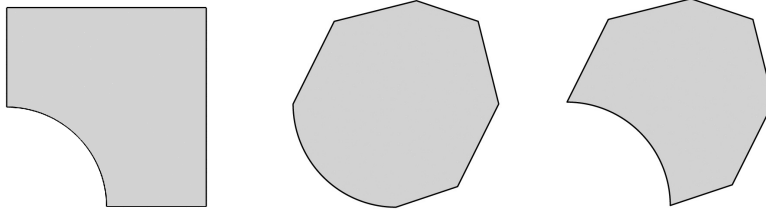


Figure 3: Some domains \mathcal{S} of polygonal type in which a side is substituted by a circular arc. In all these examples $\partial\mathcal{S}$ is locally a p -th degree NURBS curve.

5 The Tchakaloff-Davis-Wilhelmsen approach

In this paper we consider a technique based on an approach that dates back to Davis (1967) and Wilhelmsen (1976) in its general formulation, giving a constructive proof of the well-known Tchakaloff existence theorem for positive quadratures (1957).

Our strategy is based on a theorem in [38] that says the following.

Theorem 5.1 *Let be $\mathcal{F} \subset C(\mathcal{S})$ a function space of dimension k on a multi-dimensional compact set $\mathcal{S} \subset \mathbb{R}^d$ (such that \mathcal{F} contains functions that do not vanish on \mathcal{S}), $X = \{x_i\}_{i \geq 1} \subset \mathcal{S}$ an everywhere dense point sequence, and L a strictly positive linear functional on \mathcal{F} , i.e. $L(f) > 0$ for every $f \in \mathcal{F}$ not vanishing everywhere in \mathcal{S} .*

Then, for sufficiently large m , the set $X_m = \{x_1, \dots, x_m\}$ is a ‘‘Tchakaloff set’’ in \mathcal{S} , which means that, for every $f \in \mathcal{F}$, $L(f)$ can be represented as the integral with respect to a discrete positive measure with finite support in X_m of cardinality not exceeding k (i.e. as a linear combination with positive coefficients of at most k values of f in X_m).

Direct applications of the previous theorem regard the case in which $L(f)$ is an integral functional with respect to an absolutely continuous measure $w(x)dx$, i.e.

$$L(f) = \int_{\mathcal{S}} f(x) w(x) dx, \quad (26)$$

as well as w.r.t. discrete measure with support of large cardinality (for example, a positive algebraic quadrature formula or a QMC formula),

$$L(f) = \sum_{s=1}^M \lambda_s f(z_s), \quad \lambda_s > 0, \quad s = 1, \dots, M, \quad (27)$$

where $Z_M = \{z_1, \dots, z_M\} \subset \mathcal{S}$ with $M > k$.

In both instances, Theorem 5.1 ensures that for sufficiently large m there exist nodes $\{\xi_1, \dots, \xi_\nu\} \subset X_m \subset \mathcal{S}$ and corresponding positive weights $\{w_1, \dots, w_\nu\}$ such that

$$L(f) = \sum_{j=1}^{\nu} w_j f(\xi_j), \quad \nu \leq k, \quad \forall f \in \mathcal{F}. \quad (28)$$

i.e. X_m is a Tchakaloff set.

In our examples, having in mind to determine algebraic rules with a fixed degree of exactness n , we set $\mathcal{F} = \mathbb{P}_n(\mathcal{S})$, the space of multivariate polynomials of total-degree not exceeding n on \mathcal{S} . We also denote by $N = (n+1)(n+2)/2$ the dimension of the vector space $\mathbb{P}_n(\mathcal{S})$.

Aiming to a practical implementation of Tchakaloff-Davis-Wilhelmsen theorem, we proceed as follows

TDW measure compression algorithm

via moment-matching on the polynomial space $\mathbb{P}_n(\mathcal{S})$

- (i) set the moment residual tolerance tol , the starting cardinality m and the cardinality increase factor $\theta > 1$;
- (ii) select a basis $\{\varphi_1, \dots, \varphi_N\}$ of $\mathbb{P}_n(\mathcal{S})$ and compute the moments $b_j := \int_{\mathcal{S}} \varphi_j dx$, $j = 1, \dots, N$;
- (iii) generate a (quasi)-uniformly distributed sequence $X_m = \{x_1, \dots, x_m\}$ in \mathcal{S} (via an implementation of an in-domain routine over \mathcal{S});
- (iv) compute the Vandermonde-like matrix

$$V = V(X_m) = [v_{ij}] := [\varphi_j(x_i)] \in \mathbb{R}^{m \times N};$$

- (v) compute the factorization $V = QR$ with $Q \in \mathbb{R}^{m \times N}$, $R \in \mathbb{R}^{N \times N}$, and the modified moments β such that $R^t \beta = b$;
- (vi) solve the underdetermined system $Q^t u = \beta$ as a *Non-Negative Least Squares* problem

$$u^* = \operatorname{argmin} \|Q^t u - \beta\|_2, \quad u \geq 0$$

by Lawson-Hanson active-set method (see, e.g. [22] and its Matlab implementation via `lsqnonneg`, as well as its alternatives [16], [17], [18], [31]);

- (vii) if $\|V^t u^* - b\|_2 > tol$ then goto (iii) with $m := \theta m$;
- (viii) select the active weights and nodes:

$$J := \{i : u_i^* > 0\}, \quad w := u^*(J), \quad T := X_m(J).$$

A careful read of the algorithm shows that its implementation requires some key ingredients.

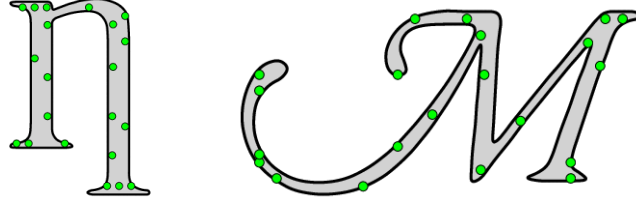


Figure 4: Rules having algebraic degree of exactness equal to 5, obtained by means of TDW measure compression algorithm, over NURBS based curvilinear polygons.

1. In (ii), once a suitable basis $\{\varphi_1, \dots, \varphi_N\}$ of $\mathbb{P}_n(\mathcal{S})$ is considered, we have to determine the moments $b_j := \int_{\mathcal{S}} \varphi_j dx$, $j = 1, \dots, N$;
2. in (iii), it is necessary to develop an in-domain routine for Jordan domains \mathcal{S} taken in consideration.

We will develop these demands in the next sections, showing in Fig. 5 the results obtained for two not trivial geometries.. For practical aspects about the choice of m and θ in (i) see [35].

6 On the moments computation

In the TDW measure compression algorithm, we have shown that once a suitable basis $\{\varphi_1, \dots, \varphi_N\}$ of $\mathbb{P}_n(\mathcal{S})$ is considered, we have to determine its moments $b_j := \int_{\mathcal{S}} \varphi_j dx$, $j = 1, \dots, N$.

In this section we develop these details, following the lines introduced in [36] and generalised in [35] to the Jordan domains mentioned above.

To this purpose, let $\mathcal{R}^* = [a_1, b_1] \times [a_2, b_2]$ be the *bounding box* of \mathcal{S} , i.e.the smallest cartesian rectangle $\mathcal{R} \supseteq \mathcal{S}$ with sides parallel to the axes. As polynomial basis $\{\varphi_j\}_{1 \leq j \leq N}$, we adopt the shifted lexicographically ordered total-degree product Chebyshev basis

$$\varphi_j(x, y) = T_{h_1}(\alpha_1(x)) \cdot T_{h_2}(\alpha_2(y)), \quad 0 \leq h_1 + h_2 \leq n$$

(where j is the position of (h_1, h_2) in such ordering) where

- $T_h(\cdot) = \cos(h \arccos(\cdot))$ is the h -degree Chebyshev polynomial of first kind;
- $\alpha_i(s) = (2s - b_i - a_i)/(b_i - a_i)$, $s \in [a_i, b_i]$, $i = 1, 2$.

The use of this basis comes from the necessity of mitigating the possible extreme ill-conditioning of Vandermonde matrices in the standard monomial basis. By Gauss-Green theorem (see e.g. [1]),

$$\gamma_j = \int_{\mathcal{S}} \varphi_j(x, y) dx dy = \oint_{\partial \mathcal{S}} \Psi_j(x, y) dy \quad (29)$$

where

$$\Psi_j(x, y) = \int \varphi_j(x, y) dx = T_{h_2}(\alpha_2(y)) \int T_{h_1}(\alpha_1(x)) dx$$

It is easy to achieve that

$$\begin{aligned} \int T_0(\alpha_1(x)) dx &= x, \\ \int T_1(\alpha_1(x)) dx &= \frac{b_1 - a_1}{4} \cdot \alpha_1^2(x), \\ \int T_h(\alpha_1(x)) dx &= \frac{b_1 - a_1}{2} \cdot \left(\frac{h}{h^2 - 1} T_{h+1}(\alpha_1(x)) - \frac{x}{h - 1} T_h(\alpha_1(x)) \right), \quad h \geq 2. \end{aligned}$$

If $P_{k,s} := (\tilde{x}(t_s^{(k)}), \tilde{y}(t_s^{(k)}))$ and $P_{k,s} \frown P_{k,s+1}$ is the arc of $\partial\mathcal{S}$ joining $P_{k,s}$ with $P_{k,s+1}$, we obtain

$$\begin{aligned} \gamma_j &= \oint_{\partial\mathcal{S}} \Psi_j(x, y) dy = \sum_{k,s} \int_{P_{k,s} \frown P_{k,s+1}} \Psi_j(x, y) dy \\ &= \sum_{k,s} \int_{t_s^{(k)}}^{t_{s+1}^{(k)}} \Psi_j(\tilde{x}(t), \tilde{y}(t)) \tilde{y}'(t) dt. \end{aligned} \quad (30)$$

The evaluation of the integrals on the r.h.s. of (30) is a delicate matter. Since \tilde{x} and \tilde{y} are in general rational functions one can use high order Gauss-Legendre rules [20], or adaptive routines as the MATLAB built-in routine `integral`, or the Extended Rational Fejèr Quadrature Rules proposed in [15].

7 The in-domain routine

In the previous section we have shown that the application of the TDW measure compression algorithm requires an in-domain algorithm for the Jordan domains \mathcal{S} taken under consideration, i.e. an algorithm that determines if $P \in \mathbb{R}^2$ is inside (or not inside) such a \mathcal{S} . This problem has been analysed in [34] and [35] and for the sake of the reader, we sketch its details below.

A well-known strategy is based on the *Jordan curve theorem* that states that a point P belongs to a Jordan domain \mathcal{S} if and only if, having taken a point $P^* \notin \mathcal{S}$ then the segment $\overline{P^*P}$ crosses $\partial\mathcal{S}$ an odd number $c(P)$ of times.

In spite of its simplicity, there can be pathological cases, e.g. when $\overline{P^*P}$ crosses a vertex or when includes a segment of $\partial\Omega$.

Another problematic situation holds when the boundary $\partial\mathcal{S}$ has a *critical* point $S = (\tilde{x}(\gamma), \tilde{y}(\gamma))$ where

$$\lim_{t \rightarrow \gamma^-} \tilde{y}'(t) \lim_{t \rightarrow \gamma^+} \tilde{y}'(t) < 0,$$

i.e. there is locally a vertical turn of boundary from left to right (or conversely from right to left). If we consider *vertical* segments $\overline{P^*P}$ then the Jordan theorem cannot be directly applied.

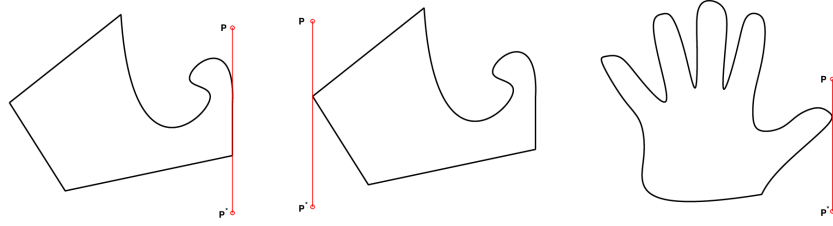


Figure 5: Critical situations for the the application of the *Jordan curve theorem* on curvilinear polygons.

These special cases, illustrated in Fig. 5, after some effort, can be classified by an algorithm, and thus we start from the most common situation that $\overline{P^*P}$ does not contain any *critical point* or vertical side.

Under these assumptions, let \mathcal{R} be a rectangle, often called *box*, with sides parallel to the cartesian axes, whose interior contains \mathcal{S} , and suppose that we have to establish if $P = (P_x, P_y)$ belongs to \mathcal{S} .

Let $P^* = (P_x^*, P_y^*)$ be the point in \mathcal{R} not internal to \mathcal{S} , such that $P_x^* = P_x$ and $P_y^* < P_y$. Geometrically it means that P^* is not internal to \mathcal{S} , shares the same abscissa of P , but is *vertically below* P .

In what follows we compute the *crossing number* $c(P)$, i.e. the number of times in which the vertical segment $\overline{P^*P}$ crosses $\partial\mathcal{S}$.

First, we cover $\partial\mathcal{S}$ with the union of possibly overlapping rectangles, each one containing a portion of $\partial\mathcal{S}$ that has no vertical turning points and is parametrized by two *rational functions*, i.e. locally $(\tilde{x}(\gamma), \tilde{y}(\gamma))$ are the ratio of two polynomials (see Fig. 6).

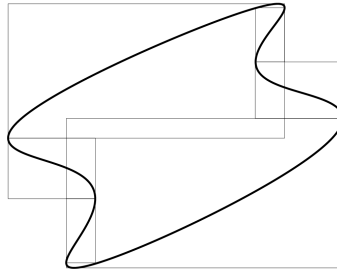


Figure 6: A Jordan domain of curvilinear type and its possibly overlapping monotone boxes.

To this purpose, we observe that since \tilde{x} , \tilde{y} are rational splines in each element $I^{(k)}$, $k = 1, \dots, M$, that takes part to the partitioning of $[a, b]$, then there are $I_j^{(k)} = [t_j^{(k)}, t_{j+1}^{(k)}] \subseteq I^{(k)}$, $k = 1, \dots, M$, $j = 1, \dots, m_k - 1$, where the

restriction of \tilde{x} , \tilde{y} to $I_j^{(k)}$ are rational functions, i.e.

$$\tilde{x}(t) = \frac{u_{k,j,1}(t)}{v_{k,j,1}(t)}, \quad \tilde{y}(t) = \frac{u_{k,j,2}(t)}{v_{k,j,2}(t)}, \quad t \in I_j^{(k)}$$

with $u_{k,j,1}$, $u_{k,j,2}$, $v_{k,j,1}$, $v_{k,j,2}$ polynomials on the interval $I_j^{(k)}$, with degree, respectively, $\eta_{k,1}$, $\eta_{k,2}$, $\delta_{k,1}$, $\delta_{k,2}$ (notice that they do not depend on j but just on the local degree of the splines $u_{k,1}$, $u_{k,2}$, $v_{k,1}$, $v_{k,2}$ in $I^{(k)}$).

If $\tilde{x} \equiv c$ in $I_j^{(k)} = [t_j^{(k)}, t_{j+1}^{(k)}]$, we set

$$\mathcal{B}_1^{(j,k)} := c \times [\min_{t \in I_j^{(k)}} \tilde{y}(t), \max_{t \in I_j^{(k)}} \tilde{y}(t)].$$

In other words, $\mathcal{B}_1^{(j,k)}$ is a box that actually consists of a vertical segment.

If \tilde{x}' has variable sign in $(t_j^{(k)}, t_{j+1}^{(k)})$, let $\mathcal{N}_j^{(k)} = \{t_i^{(j,k)}\}_{i=1, \dots, l_{j,k}}$ the set of $t_i^{(j,k)} \in (t_j^{(k)}, t_{j+1}^{(k)})$ such that $\tilde{x}'(t_i^{(j,k)}) = 0$ (as observed before, the restriction of \tilde{x} to $I_j^{(k)}$ is a rational function with the denominator nowhere null, and consequently \tilde{x}' exists), otherwise let $\mathcal{N}_j^{(k)} = \emptyset$. Next, set $T^{(j,k)} = \{t_j^{(k)}, t_{j+1}^{(k)}\} \cup \mathcal{N}_j^{(k)}$, where we suppose that its elements, say $T_i^{(j,k)}$, are in increasing order. Since $\tilde{x}(t) = u_{k,j,1}(t)/v_{k,j,1}(t)$, $t \in I_j^{(k)}$, from

$$\tilde{x}'(t) = \frac{u'_{k,j,1}(t)v_{k,j,1}(t) - u_{k,j,1}(t)v'_{k,j,1}(t)}{v_{k,j,1}^2(t)}, \quad t \in I_j^{(k)},$$

and $v_{k,j,1}^2(t) \neq 0$ for each $t \in I_j^{(k)}$, we have that $\tilde{x}'(t) = 0$ if and only if

$$u'_{k,j,1}(t)v_{k,j,1}(t) - u_{k,j,1}(t)v'_{k,j,1}(t) = 0,$$

and consequently $\mathcal{N}_j^{(k)}$ is available just solving a polynomial equation of degree $\eta_{k,1} + \delta_{k,1} - 1$.

Now define as *monotone boxes* the rectangles $\mathcal{B}_i^{(j,k)}$,

$$\mathcal{B}_i^{(j,k)} := [\min_{t \in I_i^{(j,k)}} \tilde{x}(t), \max_{t \in I_i^{(j,k)}} \tilde{x}(t)] \times [\min_{t \in I_i^{(j,k)}} \tilde{y}(t), \max_{t \in I_i^{(j,k)}} \tilde{y}(t)].$$

where $I_i^{(j,k)} := [T_i^{(j,k)}, T_{i+1}^{(j,k)}]$. By definition, if $\mathcal{N}_j^{(k)} = \emptyset$, necessarily there is only the monotone box $\mathcal{B}_1^{(j,k)}$. Since \tilde{y} is a rational function in $[T_i^{(j,k)}, T_{i+1}^{(j,k)}]$, the evaluation of

$$\min_{t \in [T_i^{(j,k)}, T_{i+1}^{(j,k)}]} \tilde{y}(t), \quad \max_{t \in [T_i^{(j,k)}, T_{i+1}^{(j,k)}]} \tilde{y}(t)$$

can be explicitly determined computing the derivative of the polynomial \tilde{y}' , its zeros in $[T_i^{(j,k)}, T_{i+1}^{(j,k)}]$ and the evaluation of \tilde{y} at $T_i^{(j,k)}$ and $T_{i+1}^{(j,k)}$.

At this point, we have determined $I_i^{(j,k)}$, such that

- the restriction of \tilde{x} , \tilde{y} to each interval $I_i^{(j,k)} \subseteq [a, b]$ are rational functions,
- \tilde{x} is a monotone function (with no turning points of $\partial\mathcal{S}$ in the interior of each $\mathcal{B}_i^{(j,k)}$),

and we are ready to apply the crossing theorem to see if $P = (P_x, P_y)$ is inside the Jordan domain \mathcal{S} .

Let

$$\mathcal{B}(P) = \{B = [\alpha_1, \beta_1] \times [\alpha_2, \beta_2] \in \mathcal{B} : P_x \in [\alpha_1, \beta_1], P_y \geq \alpha_2\}.$$

be the set that contains all the monotone boxes \mathcal{B}_l such that $\overline{P^*P} \cap \mathcal{B}_l \neq \emptyset$, and that consequently are the only ones that may contribute to the evaluation of the crossing number $c(P)$.

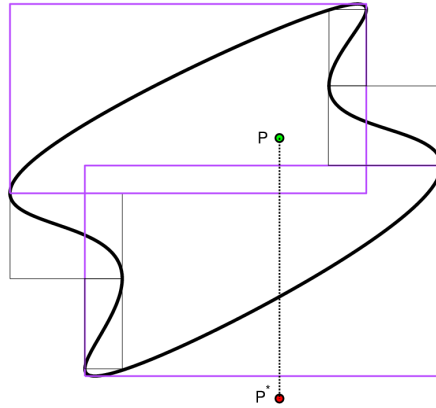


Figure 7: In magenta, the two monotone boxes useful to determine whether or not $P \in \mathcal{S}$. It is immediate to observe that the segment $\overline{P^*P}$ intersects the boundary $\partial\mathcal{S}$ just once. The monotone box *below* gives contribution 1, while the monotone box *above* gives contribution 0.

Consider one of these monotone boxes $\mathcal{B}_l = [\alpha_1^{(l)}, \beta_1^{(l)}] \times [\alpha_2^{(l)}, \beta_2^{(l)}] \in \mathcal{B}(P)$.

If $P_y > \beta_2^{(l)}$ then the point is *above the box*, and thus the segment $\overline{P^*P}$ surely crosses $\partial\mathcal{S}$ once in \mathcal{B}_l and *below* P , due to the monotonicity of \tilde{x} in \mathcal{B}_l .

Otherwise, $P \in \mathcal{B}_l$. As assumed before, $\overline{P^*P}$ is free of critical points and vertical segments of the boundary, thus \mathcal{B}_l includes a certain portion of $\partial\mathcal{S}$ described parametrically by two rational functions, say $\tilde{x}_{\mathcal{B}_l}$, $\tilde{y}_{\mathcal{B}_l}$, with arguments in the interval $I_{\mathcal{B}_l} \subseteq [a, b]$, in which $\tilde{x}_{\mathcal{B}_l}$ is monotone and such that $P_x \in \tilde{x}_{\mathcal{B}_l}(I_{\mathcal{B}_l})$. This entails that necessarily there is a unique root $t^* \in I_{\mathcal{B}_l}$ of the polynomial equation $\tilde{x}_{\mathcal{B}_l}(t) = P_x$. Since $\tilde{x}_{\mathcal{B}_l}(t) = \frac{u(t)}{v(t)}$, for suitable polynomials u , v , then t^* is the unique solution of the polynomial equation $u(t) - P_x \cdot v(t) = 0$ in $I_{\mathcal{B}_l}$.

We also observe that,

- if $\tilde{y}(t^*) < P_y$ then the segment $\overline{P^*P}$ crosses the boundary $\partial\mathcal{S}$ once in the monotone box, *below* P ;
- if $\tilde{y}(t^*) > P_y$ then the segment $\overline{P^*P}$ does not cross the boundary $\partial\mathcal{S}$ once in B , *below* P ;
- if $\tilde{y}(t^*) = P_y$ then P is on the boundary $\partial\mathcal{S}$.

After counting all the crossings, we determine whether a point P is inside or not inside the domain \mathcal{S} , by means of Jordan theorem. In Fig. 7 we illustrate by an example the contribution given by monotone boxes, while in Fig. 8 we show the results given by our procedure when applied to two complicated geometries.

When the previous assumptions do not hold, i.e. the vertical segment $\overline{P^*P}$ contains a *critical point* or a portion of a vertical side of $\partial\mathcal{S}$, one can use an algorithm based on the well-known *winding* theorem to determine if P belongs to \mathcal{S} . To this purpose, one can compute numerically the so called *winding number* $wind(P, \tilde{x}, \tilde{y}) \in \mathbb{Z}$,

$$wind(P, \tilde{x}, \tilde{y}) := \frac{1}{b-a} \int_a^b \frac{\tilde{y}'(t)(\tilde{x}(t) - P_x) - \tilde{x}'(t)(\tilde{y}(t) - P_y)}{(\tilde{x}(t) - P_x)^2 + (\tilde{y}(t) - P_y)^2} dt.$$

If the quantity $wind(P, \tilde{x}, \tilde{y})$ is odd then the point belongs to \mathcal{S} otherwise is not inside such domain.

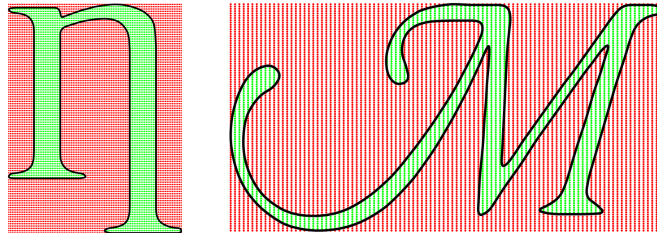


Figure 8: In-domain routine applied to grid of 10000 points on two NURBS based Jordan domains. The CPU time required for the process is respectively $2 \cdot 10^{-2}$ and $5 \cdot 10^{-2}$ seconds.

In our numerical tests, on a cloud of points, this approach is slower than the evaluation of the crossing numbers. Our experience is that for general domains the winding number strategy will only seldomly be called by the in-domain routine proposed here.

In [34] the authors take into account techniques to make the implementation efficient and safe from numerical issues. The numerical codes regarding this in-domain routine have been implemented in Matlab and are freely available at [32].

8 Numerical tests

This section presents numerical tests to validate the proposed curvilinear VEM methodology for the homogenization of fibre-reinforced composite materials. In particular, in Section 8.1 we show a set of simple patch tests on a fictitious square domain with a minimal mesh comprising variously distorted curvilinear polygons. In Section 8.2 we perform asymptotic homogenization for the basic case of doubly periodic composite materials with complex fibre shapes. Finally, in Section 8.3 we address a real scale engineering problem i.e. computational homogenization of composite materials with randomly distributed highly complex unidirectional fibres, applying Monte Carlo simulations to obtain statistically averaged effective properties.

8.1 Patch test

In this section we assess accuracy and robustness through representative boundary value problems on a unit square domain with known solution i.e. patch tests with a linear solution in terms of the cell function χ . The domain is represented by a unit square and meshes with the lowest number of curvilinear quadrilaterals both convex and concave (see Fig. 9 and Fig. 10) which are also progressively distorted by moving the inner curvilinear polygon which is characterized by having the whole boundary as a sequence of circular arches. The problem is split in two cases for each examined mesh configuration, namely applying a unit shear strain e_s ($s = 1, 2$) along the y_1 and y_2 direction (see Eq. (10)), respectively, and solving the ensuing homogenized equilibrium equation, Eq. (24), for each loading condition.

Numerical results in terms of H^1 error measure on the cell function are reported in Table 1, which shows that the proposed methodology exactly solve a general \mathcal{P}_1 -type patch test with no major sensitivity to mesh distortion.

8.2 Doubly periodic composites

In order to verify the capability of the method to tackle complex curvilinear fibre shape in efficient manner, we here study doubly periodic fibre-reinforced composites for different fibre arrangements and material setups. A given doubly periodic composite unit cell is identified through the geometrical features φ , $\kappa = L_2/L_1$, f , and the following dimensionless material parameters:

- fibre/matrix stiffness ratio (contrast factor) $\xi = G^f/G^m$;
- dimensionless interface parameter $\delta = D/(G^m L_1)$;

The simulations refer to square RUC for simplicity i.e. $\varphi = \pi/2$, and $\kappa = 1$. The first benchmark corresponds to elliptic cross section inclusions for $f = 0.1, 0.2, 0.4$, respectively, as can be see in Fig. 11, perfect interfaces i.e. $\delta = \infty$ and a contrast factor $\xi = 50$. The inclusions scale homothetically, with a constant ratio between semi-axes fixed at $2/3$. For each computational domain

geometry, quadrilateral mesh discretizations are still adopted. Representative meshes of a quarter of the domain are portrayed in Fig. 11, in view of the double symmetry offered by all three cases. Presented results are obtained for five mesh sizes applying uniform refinement. Lacking a closed form or semi-analytical solution for the case under investigation, as reference results we use standard Lagrangian quadrilateral quadratic finite elements with an overkilling mesh resolution.

In Fig. 12 we report h -convergence plots for the cell function $\chi(y)$ in the H^1 -error norm for uniform mesh refinement, for the set of examined volume fractions.

The expected convergence rate is linear which is obtained for all examined patterns. We notice that the exact geometric representation of the curved interface produce accurate results in conjunction with the implemented NURBS quadrature formula. It is moreover observed that progressively higher volume fractions of fibres require higher computational cost to reach a given accuracy level. The second doubly periodic composite under investigation still regards a complex fibre boundary which, differing from the previous case, exhibits a re-entrant sharp corner. The RUC domain is represented in Fig. 13 indicating still a square RUC which lodges a bilobe-type inclusion made of two circular fibres with the same radius fused together with an overlapping of a third of the radial length. Due to symmetry a quarter of the domain is meshed as can be inspected in Fig. 13. We examine two sets of problems for a fixed volume fraction $f = 0.2$. First, we consider perfect interfaces ($\delta = \infty$) and values of stiffness ratio $\xi = 10, 100, 1000$, respectively. Subsequently, we fix $\xi = 100$ and analyze the following values for the interface integrity indicator: $\delta = 10, 100, 1000, \infty$.

Optimal (linear) convergence rate for all cases is observed in Fig. 14 where H^1 -error plots are obtained through uniform mesh refinement sequence. This further set of results confirms method consistency and capability of exactly representing the curvilinear interface geometry. An additional improvement which would furtherly enhance the computational performance of the methodology is adaptive mesh refinement, guided by an efficient and reliable error estimator procedure, which in principle would indicate localization of the error (hence local refinement) at fibre/matrix interface, and at unit cell boundary edges (see [5] for a thorough presentation of the method).

8.3 Random composites with stochastically distributed inclusions

The engineering relevant case of random composites relies on a statistical homogenization approach which for instance amounts to solving for large number of RUC random realizations and subsequently infer homogenized material properties through statistical averaging of the results [25, 19]. In this context, one key assumption is to consider statistically homogeneous randomly generated microstructures, yielding an isotropic effective behaviour [19]. It is known that with this aim, quantitative estimation of the RUC size plays an important role from accuracy and computational cost point of view, since the effective mod-

ulus $G^\#$, obtained by Eq. (14) is actually a random variable depending on the realizations of the RUC D examined throughout the statistical homogenization procedure. The main problem is then to determine a proper RUC size to guarantee a prescribed accuracy on the effective material moduli. The idea is then not to use too large RUCs requiring heavy computational effort, instead, sampling a higher number of smaller RUCs setups to get a prefixed accuracy [19]. To this end, in this context where we focus specifically on solving complex curvilinear fibre cross sections, we apply the statistical homogenization procedure presented recently in [5] in a simplified form, i.e. with standard uniform mesh refinement.

As a manufactured benchmark we present numerical simulations on four geometrical arrangements of square RUCs with equal, homogeneous isotropic trilobe-shaped fibres with volume fraction $f = 0.2$, stiffness ratio $\xi = 1000$, $\delta = \infty$. The RUC-to-fibre number ratio ranges from 2 to 16, see Fig. 15 for a pictorial representation of such four typical realizations and relevant quadrilateral meshes. Fibre cross section profiles are no more axis-symmetric, and are obtained blending three elliptical arcs with as many circular fillets granting smoothness of the overall boundary. Each ellipse has semi-axes ratio $2/5$, while the ratio between circular arcs radius and minimal elliptical semi-axis is fixed in order to match the prescribed volume fraction of the composite.

The idea is then to solve a sufficiently large number n of realizations with a standard uniform mesh refinement strategy and numerically assess the statistics of result distribution. We refer to [5] for a more detailed description of the computational homogenization procedure based on Monte Carlo simulations.

Fig. 16 shows the normalized mean value $\mu_{G^\#}/G^m$ and the dispersion of $G^\#$ as a function of the number of trilobe inclusions per RUC. As it is expected, larger RUCs are associated to higher accuracy and lower dispersion and hence can be used to obtain a fair estimate of $\mu_{G^\#}$.

9 Conclusion

In this communication, we have addressed the computational asymptotic homogenization of reinforced composite materials with long parallel fibres having a complex curvilinear cross section. An augmented VEM formulation, based on the conjoined use of an efficient quadrature formula for NURBS-type curvilinear polygons and an augmented projection space, has been developed for the effective computational analysis of the above class of heterogeneous materials in the framework of antiplane deformation. VEM has been recently developed as a generalization of the Finite Element Method (FEM) and it allows the use of curvilinear polygonal elements of general, including non-convex elements. The proposed method has been validated through an extensive numerical campaign showing its generality for modelling accurately multiphase complex material. Further research aims at extending the method to include material non-linear behaviour and damage.

Table 1: Curvilinear VEM patch tests H^1 -error measures on χ .

	shear dir.	sym	rot	trsl	dist
mesh S-cnv	$-y_1$	1.6710e-15	1.4492e-15	2.7327e-15	2.0848e-15
	$-y_2$	7.3042e-15	1.3048e-14	2.1801e-15	7.7697e-15
mesh S-cnc	$-y_1$	2.7826e-15	1.7097e-15	1.4332e-15	2.0231e-15
	$-y_2$	2.5073e-15	5.3894e-15	4.3447e-15	1.8341e-14

Acknowledgements

Work partially supported by the DOR funds and the biennial project BIRD 192932 of the University of Padova, by the INdAM-GNCS 2022 Project “*Methods and software for multivariate integral models*” and by the INdAM-GNCS 2023 Project “*Approximation and multivariate integration, with application to integral equations*”. This research has been accomplished within the RITA “*Research ITalian network on Approximation*”, the “ANA&A SIMAI” group and within the UMI Group TAA “*Approximation Theory and Applications*” (A. Sommariva).

References

- [1] T.M. Apostol, *Calculus*, 2nd ed., vol. II, Blaisdell, 1969.
- [2] E. Artioli, L. Beirão da Veiga, C. Lovadina, E. Sacco, Arbitrary order 2D virtual elements for polygonal meshes: Part I, elastic problem, *Computational Mechanics* 60 (2017) 355–377.
- [3] E. Artioli, Asymptotic homogenization of fibre-reinforced composites: a virtual element method approach, *Meccanica* 53 (2018) 1187–1201.
- [4] E. Artioli, L. Beirão da Veiga and F. Dassi, Curvilinear Virtual Elements for 2D solid mechanics applications, *Comput. Methods Appl. Mech. Eng.*, 35 (2020), 112667.
- [5] E. Artioli, L. Beirão da Veiga, M. Verani, An adaptive curved virtual element method for the statistical homogenization of random fibre-reinforced composites, *Finite Elements in Analysis and Design*, 177, (2020), 103418.
- [6] E. Artioli, A. Sommariva and M. Vianello, Algebraic cubature on polygonal elements with a circular edge, *Comput. Math. Appl.*, 79 (2020), 2057–2066.
- [7] L. Beirão da Veiga, F. Brezzi, A. Cangiani, G. Manzini, L.D. Marini, and A. Russo. Basic principles of virtual element methods. *Mathematical Models and Methods in Applied Sciences*, 23(01):199–214, 2013.

- [8] L. Beirão da Veiga, F. Brezzi, L. D. Marini, A. Russo, The hitchhiker’s guide to the virtual element method, *Math. Models Methods Appl. Sci.* 24 (08) (2014) 1541–1573.
- [9] L. Beirão da Veiga, A. Russo, G. Vacca, The virtual element method with curved edges, *ESAIM: Math. Mod. Numer. Anal.* 53 (2) (2019) 375–404.
- [10] L. Beirão da Veiga, F. Brezzi, L.D. Marini, and A. Russo. Polynomial preserving virtual elements with curved edges. *Mathematical Models and Methods in Applied Sciences*, 30(08):1555–1590, 2020.
- [11] A. Bensoussan, J. Lions, G. Papanicolau, Asymptotic Analysis for Periodic Structures, North-Holland, Amsterdam, 1978.
- [12] D. Bigoni, S. K. Serkov, M. Valentini, A. B. Movchan, Asymptotic models of dilute composites with imperfectly bonded inclusions, *Int. J. Solids Struct.* 35 (24) (1998) 3239–3258.
- [13] P. J. Davis, A construction of nonnegative approximate quadratures, *Math. Comp.*, 21 (1967), 578–582.
- [14] C. de Boor, A Practical Guide to Splines, Rev.ed. Springer-Verlag, New York, 2001.
- [15] K. Deckers, A. Mougaida, and H. Belhadjsalah Algorithm 973: Extended Rational Fejér Quadrature Rules based on Chebyshev Orthogonal Rational Functions, *ACM Transactions on Mathematical Software*, 43-4 (2017), 1–29.
- [16] M. Dell’Orto, M. Dessole, F. Marcuzzi, The Lawson-Hanson Algorithm with Deviation Maximization: Finite Convergence and Sparse Recovery, *Numer. Linear Algebra Appl.*, 30 (2023), e2490.
- [17] M. Dessole, F. Marcuzzi, M. Vianello: dCATCH: a numerical package for d-variate near G-optimal Tchakaloff regression via fast NNLS, *MDPI-Mathematics*, 8(7) (2020), 1122 - Special Issue “Numerical Methods”.
- [18] M. Dessole, F. Marcuzzi, M. Vianello, Accelerating the Lawson-Hanson NNLS solver for large-scale Tchakaloff regression designs, *Dolomites Res. Notes Approx. DRNA*, 13 (2020), 20–29.
- [19] T. Kanit, S. Forest, I. Galliet, V. Mounoury, D. Jeulin, Determination of the size of the representative volume element for random composites: statistical and numerical approach, *Int. J. Solids Struct.* 40 (2003) 3467–3679.
- [20] N. Hale and A. Townsend, Fast and Accurate Computation of Gauss-Legendre and Gauss-Jacobi Quadrature Nodes and Weights, *SIAM J. Sci. Comput.*, 35-2 (2013), A652:A674.
- [21] Z. Hashin, The spherical inclusion with imperfect interface, *J. Appl. Mech.* 58 (1991) 444–449.

- [22] C. L. Lawson, R. J. Hanson, Solving least squares problems, Classics in Applied Mathematics 15, SIAM, Philadelphia, 1995.
- [23] F. Lene, D. Leguillon, Homogenized constitutive law for a partially cohesive composite material, *Int. J. Solids Struct.* 18 (1982) 443–458.
- [24] L. Mascotto, The role of stabilization in the virtual element method: a survey, *Comput. Math. Appl.* 151 (2023) 244–251.
- [25] M. Ostoja-Starzewski, Material spatial randomness: From statistical to representative volume element, *Probabilistic Engineering Mechanics* 21 (2) (2006) 112 – 132.
- [26] L. Piegl, The NURBS Book, Second Edition, Springer-Verlag, Berlin-Heidelberg, 1997.
- [27] M. Pingaro, E. Reccia, P. Trovalusci, R. Masiani, Fast statistical homogenization procedure (FSHP) for particle random composites using virtual element method, *Comp. Mech.* 64 (2019) 197–210.
- [28] E. Sanchez-Palencia, Comportements local et macroscopique d’un type de milieux physiques heterogenes, *Int. J. Eng. Sci.* 12 (1974) 331–351.
- [29] E. Sanchez-Palencia, Non-Homogeneous Media and Vibration Theory, Lecture notes in physics, Springer, Berlin, 1980.
- [30] R. Sevilla, S. Fernández-Méndez, Numerical integration over 2D NURBS-shaped domains with applications to NURBS-enhanced FEM *Finite Elements in Analysis and Design*, 47-10 (2011), 1209–1220.
- [31] M. Slawski, Non-negative least squares: comparison of algorithms, available at <https://sites.google.com/site/slawskimartin/code>.
- [32] A. Sommariva, inRS, indomain routines for NURBS, composite Bezier or bivariate parametric splines domains, available at <https://github.com/alvisesommariva/inRS>.
- [33] A. Sommariva, CUB_RS: MATLAB toolbox for algebraic cubature on NURBS-shaped domains, available at https://github.com/alvisesommariva/CUB_RS.
- [34] A. Sommariva, M. Vianello, inRS: implementing the indicator function for NURBS-shaped planar domains *Applied Mathematics Letters*, Volume 130, August 2022, 108026.
- [35] A. Sommariva, M. Vianello, Low cardinality Positive Interior cubature on NURBS-shaped domains, *BIT Numer. Math.*, Volume 63, article 22 (2023)
- [36] A. Sommariva, M. Vianello, Computing Tchakaloff-like cubature rules on spline curvilinear polygons, *Dolomites Res. Notes Approx.*, 14 (2021), 1-11.

- [37] V. Tchakaloff, Formules de cubatures mécaniques à coefficients non négatifs, (French) *Bull. Sci. Math.*, 81 (1957), 123–134.
- [38] D. R. Wilhelmsen, A Nearest Point Algorithm for Convex Polyhedral Cones and Applications to Positive Linear approximation, *Math. Comp.*, 30 (1976), 48–57.

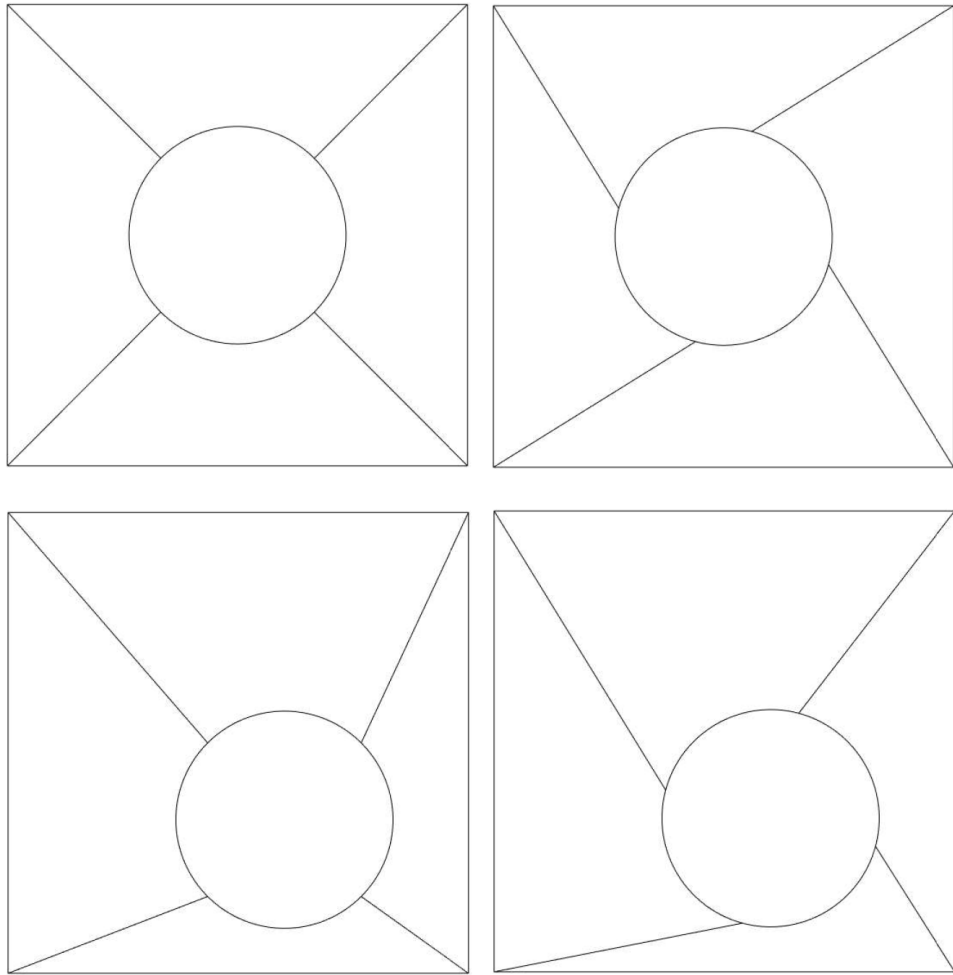


Figure 9: Patch test on a unit square domain. Minimal curvilinear polygon meshes comprising a quadrilateral with four convex circular edges with same radius and four quadrilaterals with one concave circular edge. Meshes are progressively distorted through shift and rotation of inner polygon.

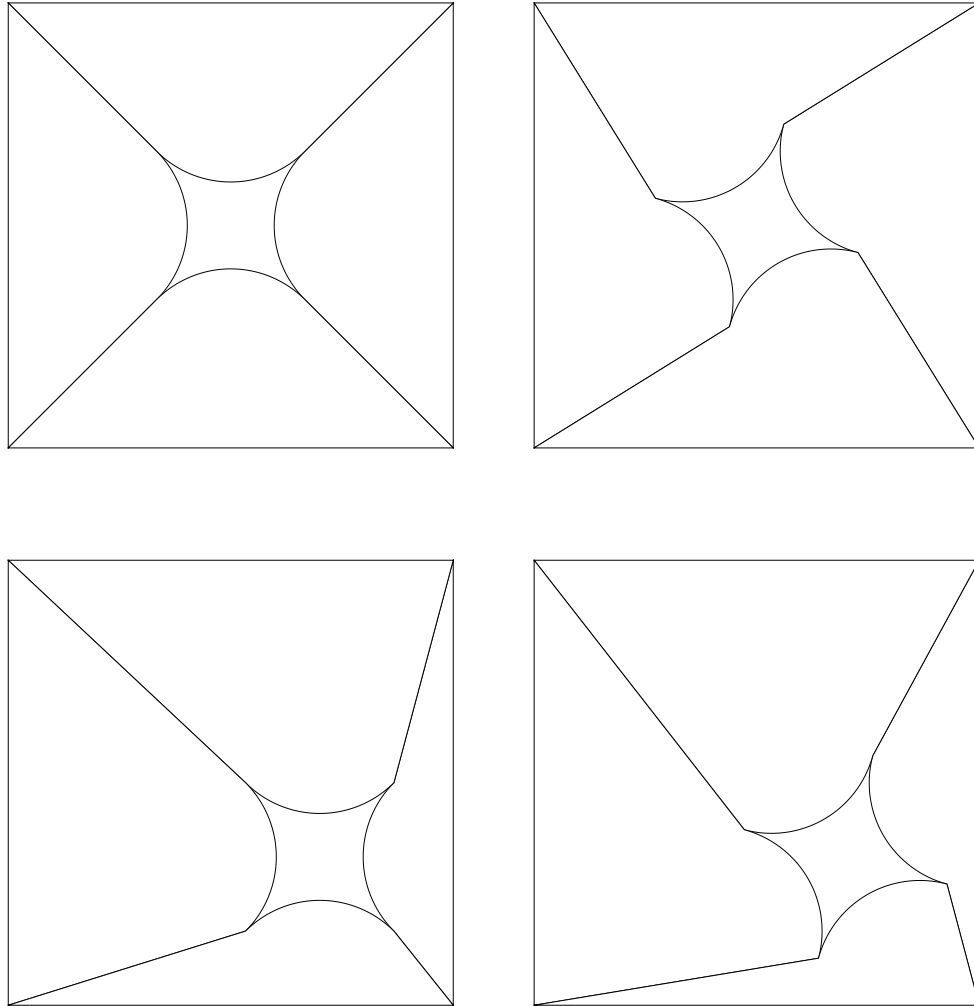


Figure 10: Patch test on a unit square domain. Minimal curvilinear polygon meshes comprising a quadrilateral with four concave circular edges with same radius and four quadrilaterals with one convex circular edge. Meshes are progressively distorted through shift and rotation of inner polygon.

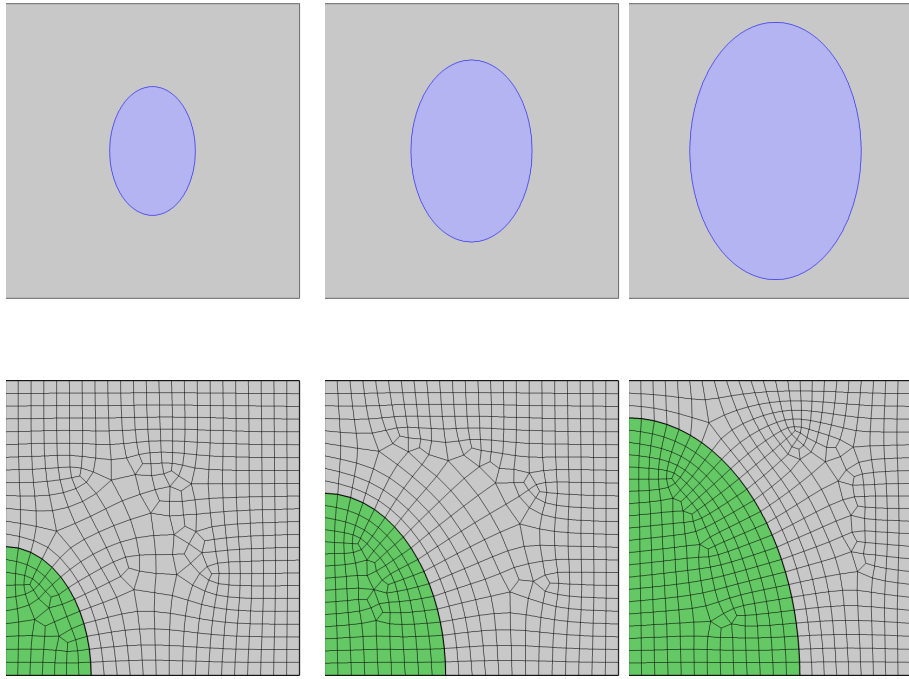


Figure 11: Asymptotic homogenization of doubly periodic composite material with elliptical inclusions. Square RUC, volume fraction $f = \{0.1, 0.2, 0.4\}$ (*upper panel*), stiffness contrast factor $\xi = 50$, perfect interface s.t. $\delta = \infty$. Curvilinear quadrilateral meshes of a relevant quarter of domain due to double symmetry with respect to (y_1, y_2) axes (*lower panel*). Elliptical inclusion semi-axis ratio equal to $2/3$.

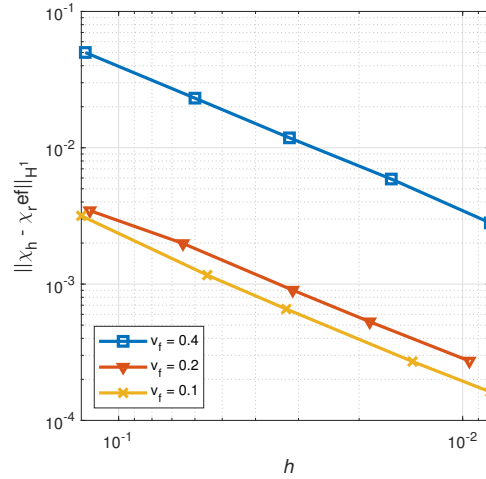


Figure 12: Asymptotic homogenization of doubly periodic composite material with elliptical inclusions. h -convergence in the H^1 error norm on the cell function χ .

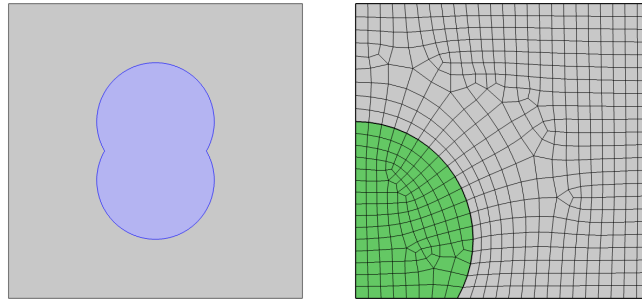


Figure 13: Asymptotic homogenization of doubly periodic composite material with complex bi-lobe inclusions. Square RUC, volume fraction $f = 0.2$ (*left panel*), stiffness contrast factor $\xi = \{10, 100, 1000\}$, interface parameter $\delta = \{10, 100, 1000, \infty\}$. Curvilinear quadrilateral meshes of a relevant quarter of domain due to double symmetry with respect to (y_1, y_2) axes (*right panel*). Bilobed inclusion made up of two circular fibres with a geometric overlapping of a third of radius.

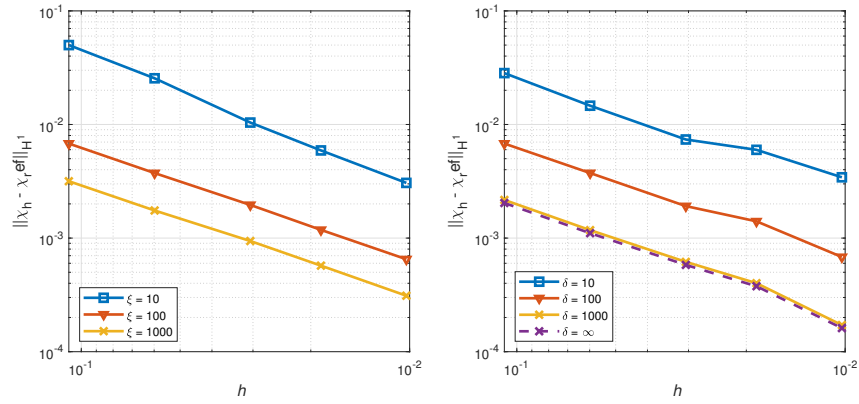


Figure 14: Asymptotic homogenization of doubly periodic composite material with complex bi-lobe inclusions. h -convergence in the H^1 error norm on the cell function χ for varying stiffness contrast factor ξ (left panel), and varying interface parameter δ (right panel).

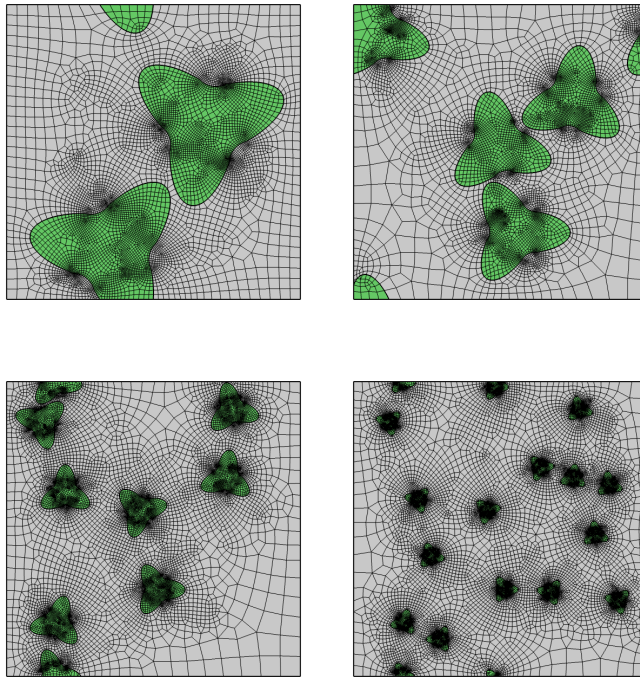


Figure 15: Statistic homogenization of a composite with randomly distributed fibres with complex curvilinear cross section geometry. Stochastic realization of a square RUC of a composite with prescribed volume fraction $f = 0.2$ and respectively 2, 3, 4, 16 complex shaped trilobed fibres: conforming curvilinear quadrilateral meshes.

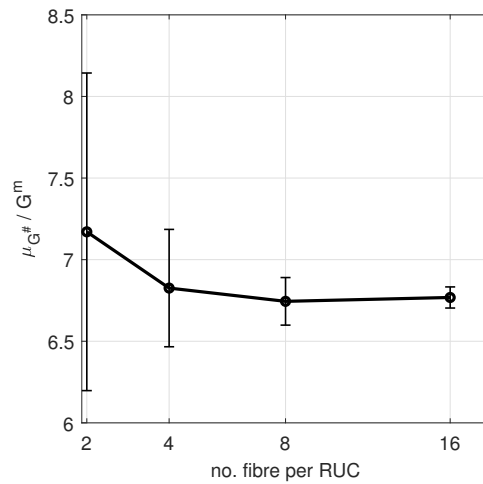


Figure 16: Statistic homogenization of a composite with randomly distributed fibres with complex curvilinear cross section geometry. Mean value $\mu_{G^{\#}}$ and dispersion of $G^{\#}$, normalized by G^m as a function of the number of trilobe inclusion per RUC obtained through Monte Carlo simulation; fibre/matrix stiffness ratio $\xi = 1000$. , perfect interface ($\delta = \infty$).